

Calmodulin Regulates Ca^{2+} -sensing Receptor-mediated Ca^{2+} Signaling and Its Cell Surface Expression^{*[5]}

Received for publication, May 24, 2010, and in revised form, July 27, 2010 Published, JBC Papers in Press, September 8, 2010, DOI 10.1074/jbc.M110.147918

Yun Huang^{†1}, Yubin Zhou^{†1}, Hing-Cheung Wong[‡], Adriana Castiblanco[‡], Yanyi Chen[‡], Edward M. Brown[§], and Jenny J. Yang^{‡2}

From the [†]Department of Chemistry, Center for Drug Design and Advanced Biotechnology, Georgia State University, Atlanta, Georgia 30303 and the [§]Department of Medicine, Division of Endocrinology, Diabetes and Hypertension, Brigham and Women's Hospital, Boston, Massachusetts 02115

The Ca^{2+} -sensing receptor (CaSR) is a member of family C of the GPCRs responsible for sensing extracellular Ca^{2+} ($[\text{Ca}^{2+}]_o$) levels, maintaining extracellular Ca^{2+} homeostasis, and transducing Ca^{2+} signaling from the extracellular milieu to the intracellular environment. In the present study, we have demonstrated a Ca^{2+} -dependent, stoichiometric interaction between CaM and a CaM-binding domain (CaMBD) located within the C terminus of CaSR (residues 871–898). Our studies suggest a wrapping around 1–14-like mode of interaction that involves global conformational changes in both lobes of CaM with concomitant formation of a helical structure in the CaMBD. More importantly, the Ca^{2+} -dependent association between CaM and the C terminus of CaSR is critical for maintaining proper responsiveness of intracellular Ca^{2+} responses to changes in extracellular Ca^{2+} and regulating cell surface expression of the receptor.

Ca^{2+} -sensing receptors (CaSRs)³ represent a class of receptors that function as the “thermostats” of the body for monitoring and regulating the extracellular calcium concentration ($[\text{Ca}^{2+}]_o$), thereby playing a central role in the control of $[\text{Ca}^{2+}]_o$ homeostasis (1, 2). Nearly 200 mutations and polymorphisms have been identified in the CaSR. Inactivating CaSR mutations detected in patients with familial hypocalciuric hypercalcemia and neonatal severe hyperparathyroidism have been reported to cause reduced sensitivity of the receptor to $[\text{Ca}^{2+}]_o$, whereas a number of activating mutations found in

patients with autosomal dominant hypoparathyroidism lead to enhanced sensitivity toward $[\text{Ca}^{2+}]_o$ (3). Therefore, CaSR serves as an important therapeutic target in disorders associated with abnormal $[\text{Ca}^{2+}]_o$ homeostasis. CaSR belongs to family C of the superfamily of G protein-coupled receptors (GPCR), which includes metabotropic glutamate receptors (mGluRs), GABA_B receptors, pheromone receptors, and taste receptors. The amino acid sequence of CaSR remains well conserved across different species, including human, bovine, rabbit, and rat, as well as in birds, amphibians, and fish. Human CaSR contains a large extracellular domain (612 amino acid residues), a seven-transmembrane domain with 250 amino acids, and a 216-residue carboxyl-terminal C-tail. The presence of naturally occurring mutations in the C terminus of CaSR in patients with familial hypocalciuric hypercalcemia, neonatal severe hyperparathyroidism, and autosomal dominant hypocalcemia supports its functional importance (4).

Like other GPCRs, CaSR is capable of transducing extracellular signals across the plasma membrane via various G proteins (e.g. $\text{G}\alpha_i$, $\text{G}\alpha_q$, and $\text{G}\alpha_{12/13}$) (5) to regulate intracellular responses. CaSR interacts with various intracellular proteins to carry out its unique functions in specific cell types and tissues through its flexible intracellular regions (6). Among these, the 216-residue C-tail has been reported to interact with a number of proteins, including filamin-A (7), potassium channels (8), and E3 ubiquitin ligase (9). Furthermore, previous studies have shown that truncations at the C terminus of CaSR can cause either loss- or gain-of-function of the receptor. Activation of the CaSR is coupled to changes in various intracellular signaling systems, and increases in the cytosolic Ca^{2+} concentration ($[\text{Ca}^{2+}]_i$) are frequently monitored to assess the activity of the receptor. For example, truncation at residues 874 (10) or 876 (11) results in loss of responsiveness to $[\text{Ca}^{2+}]_o$, whereas truncation between 895 and 1075 causes overreactivity of CaSR toward $[\text{Ca}^{2+}]_o$ (12). Taken together, these findings strongly indicate that the sequence between 874 and 895 in the C terminus of CaSR is crucial for proper intracellular signaling cascades in response to external stimuli.

Several lines of evidence show that the CaSR and mGluRs share similar structural features and sensitivities to agonists (e.g. divalent and trivalent cations), although the sequence identities of the CaSR and mGluRs are low (~27%) (13). Furthermore, CaSR and the mGluRs share common interacting partners at similar regions of their C-tails. For example, filamin-A has been reported to interact with both mGluR7b from amino

^{*} This work was supported, in whole or in part, by National Institutes of Health Grants GM62999-1 and GM081749-01 (to J. J. Y.) and DK078331 (to E. M. B.), National Science Foundation Grant MCB-0092486, American Heart Association Grant 0655168B (to J. J. Y.), a predoctoral fellowship from the Brain and Behavior Program at Georgia State University (to Y. H.), and a predoctoral fellowship from the Molecular Basis of Disease at Georgia State University (to Y. Z.).

[5] The on-line version of this article (available at <http://www.jbc.org>) contains supplemental “Methods,” Table S1, and Figs. S1–S5.

¹ Both authors contributed equally to this study.

² To whom correspondence should be addressed: University Plaza, Atlanta, GA 30303. Tel.: 404-651-4620; Fax: 404-651-2751; E-mail: chejy@langate.gsu.edu.

³ The abbreviations used are: CaSR, Ca^{2+} -sensing receptor; CaM, calmodulin; aa, amino acid(s); RDC, residual dipolar coupling; ITC, isothermal titration calorimetry; mGluR, metabotropic glutamate; MES, 4-morpholineethanesulfonic acid; BisTris, 2-[bis(2-hydroxyethyl)amino]-2-(hydroxymethyl)propane-1,3-diol; dansyl, 5-dimethylaminonaphthalene-1-sulfonyl; CaMBD, CaM-binding domain; HSQC, heteronuclear single quantum coherence; PDB, protein data bank.

acids 909–918 (14) and CaSR from residues 962–981 (7). Betz and co-workers (15) have mapped a calmodulin (CaM)-binding region in the C terminus of mGluR7a, and they have reported that CaM competes with Gβγ for binding to the C terminus of mGluR7a, which, in turn, activates P/Q-type Ca²⁺ channels and inhibits glutamate release (15). Meanwhile, CaM dynamically regulates the trafficking of mGluR5 and directly modulates phosphorylation at Ser-901 by PKC (16). In the present study, we report for the first time the prediction of a CaM-binding region in the C terminus of CaSR and then characterize the Ca²⁺-dependent interaction between CaM and this region (aa 874–892) by using peptide models combined with fluorescence, circular dichroism (CD), and nuclear magnetic resonance (NMR) spectroscopy. In addition, we show that this Ca²⁺-dependent interaction plays an important role in the maintenance of proper responsiveness to alteration in [Ca²⁺]_o, due, at least in part, to preservation of higher levels of the receptor on the cell surface.

MATERIALS AND METHODS

Peptide and Proteins—The CaM target data base was used to predict the potential CaM-binding domain in CaSR (17). A peptide corresponding to the predicted CaMBD (Ac-⁸⁷¹-VRCSTAAHAFKVAARATLRRSNVSRKR⁸⁹⁸-NH₂) was synthesized by AnaSpec with a purity of >80%. The predicted CaM-binding site (TIEEVRCSTAAHAFKVAARATLRRSNVSRKRSSS) in the C-tail region of CaSR was engineered into the pGEX-2T vector following the BamHI restriction site with a GGG linker (denoted as GST-CaMBD). Six truncated and site-directed mutations were made in intact CaSR and GST fusion protein using PCR as described previously (18). T888V, T888E (3E1), F881E/T888E (3E2), F881E/T888V/V894E (3E2V), F881E/T888E/V894E (3E3), and deletion of Ala-880 to Val-894 (deletion) were introduced as shown in Fig. 1.

NMR Spectroscopy—¹H-¹⁵N-HSQC data were collected with a Varian INOVA 600 MHz NMR spectrometer at 37 °C. Each sample of 0.3 mM uniformly ¹⁵N-labeled CaM was placed in a buffer consisting of 5 mM MES, 10 mM BisTris (pH 6.5), 5 mM DTT, 0.1 mM Na₂N₃, 10 mM CaCl₂, and 10% D₂O. The sample was titrated against a peptide stock solution in the same buffer. NMR data were processed using NMRpipe and analyzed using Sparky. Chemical shift perturbations (Δ) of the ¹H-¹⁵N spectra with and without peptide were calculated using both ¹H and ¹⁵N chemical shifts (δ) as shown in Equation 1.

$$\Delta\delta = \sqrt{\frac{(\Delta\delta^1H)^2 + \left(\frac{\Delta\delta^{15}N}{5}\right)^2}{2}} \quad (\text{Eq. 1})$$

Residual dipolar coupling (RDC) measurements were performed on a Varian 800 MHz spectrometer using a 0.5 mM ¹⁵N-labeled CaM in complex with the CaSR peptide (1:2). First, the ¹H-¹⁵N isotropic couplings of the complex were measured by a TROSY-based J-modulation experiment (19). The complex was placed into Pf1 phage medium, and the couplings were measured again. Then RDC were obtained by subtracting the isotropic couplings from the values measured in the second

experiment. RDC data were analyzed, and structures deposited in the PDB were fit to the experimentally measured couplings using the program REDCAT (20).

Isothermal Titration Calorimetry (ITC)—ITC experiments were carried out on a Microcal VP-ITC microcalorimeter at 25 °C by following previously described procedures (21). In brief, samples were dissolved in a degassed buffer consisting of 20 mM HEPES, 150 mM KCl, 1 mM CaCl₂ (pH 7.5). The injector syringe was loaded with 400–800 μM CaM, and the sample cell contained 20–40 μM synthetic peptides. For each titration point, 6–10 μl of CaM was injected into the cell. The heat of dilution and mixing was measured in control experiments and subtracted. The experiment was repeated three times and the acquired data were analyzed using the Microcal Origin software as described previously (21).

Fluorescence Spectroscopy and the Measurement of [Ca²⁺]_i by Fluorimetry in Cell Populations—Fluorescence spectra were recorded using a PTI fluorimeter at 25 °C. The fluorescence emission spectrum of dansyl-CaM and anisotropy measurements upon complex formation were carried out as previously described (21) (see supplemental “Methods” for details).

Measurement of [Ca²⁺]_i in cell populations was performed using CaSR-transfected HEK293 cells loaded with Fura-2/AM in 20 mM HEPES, containing 125 mM NaCl, 5 mM KCl, 1.25 mM CaCl₂, 1 mM MgCl₂, 1 mM NaH₂PO₄, 1% glucose, and 1% BSA (pH 7.4) for 2 h at 37 °C and then washed once with 20 mM HEPES pH 7.4, containing 125 mM NaCl, 5 mM KCl, 0.5 mM CaCl₂, 0.5 mM MgCl₂, 1% glucose, and 1% BSA (bath buffer). HEK293 cells were transiently transfected with WT or mutant CaSRs for 48 h when cells reached 50% confluence. By the time the fluorescence experiments were carried out, the transfected cells had reached ~90% confluence. The coverslips with transfected, and Fura-2-loaded HEK293 cells were placed diagonally in 3-ml quartz cuvettes containing bath buffer. The fluorescence spectra at 510 nm was measured during stepwise increases in the extracellular calcium concentration with alternating excitation at 340 and 380 nm. The ratio of the emission at 510 nm when excited at 340 or 380 nm was used to calculate [Ca²⁺]_i. The EC₅₀ and Hill constants were fitted using the Hill equation.

CaSR Internalization Assay Using Dual Color Labeling Method—For internalization experiments, cell surface CaSR was stained with monoclonal anti-CaSR antibody (Abcam) for 1 h at 4 °C. The cells were then treated with varying levels of [Ca²⁺]_o for 2 h at 37 °C. Un-internalized CaSR was labeled with Alexa Fluor® 555-conjugated goat anti-mouse IgG. Cells were then permeabilized with 1% Triton-X100 and internalized CaSR was stained with FITC-conjugated anti-mouse IgG. The images were obtained using a Leica DM6000 fluorescence microscope and a Zeiss 510 laser scanning microscope. To quantify the extent of CaSR internalization, a similar protocol was used. 10⁶ cells were collected and the fluorescence intensity was measured using FACS. The percentage of internalized CaSR was calculated by using fluorescence intensity from internalized receptor divided by the total fluorescence intensity.

CaSR Internalization Detected with Cleavable Biotin Assay—Surface CaSR were labeled with 30 μg/ml of disulfide-cleavable biotin for 30 min at 4 °C and then stimulated with 4 mM Ca²⁺

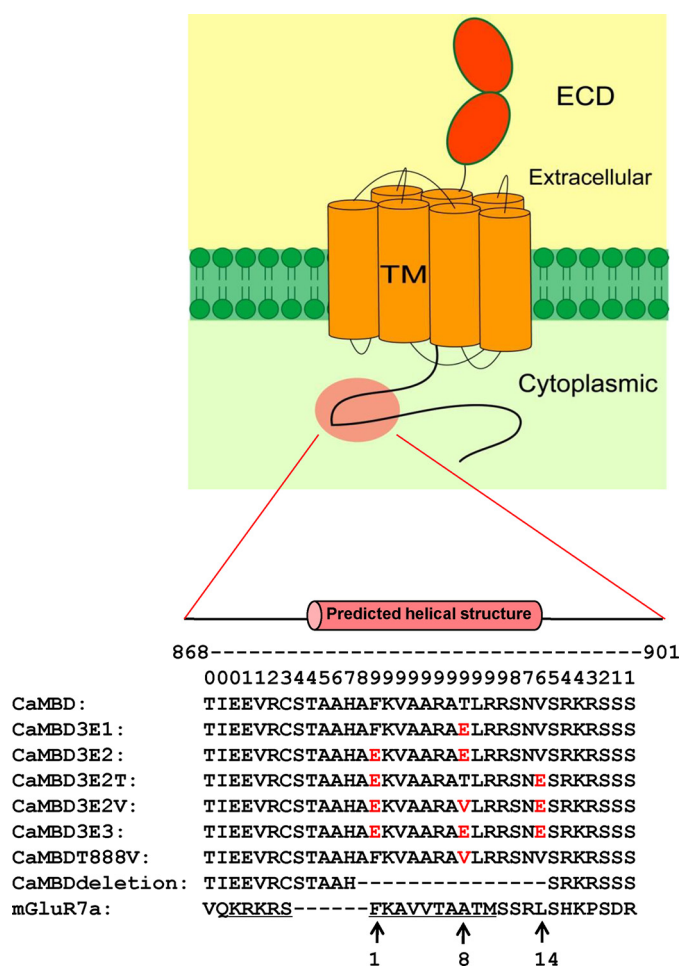


FIGURE 1. The sequence of a putative CaMBD in CaSR and design of mutants predicted to interfere with its interaction with CaM. The prediction scores, ranging from 1 to 9, represent the probability of an accurate prediction of a high affinity CaM-binding site. 3E1 contains the mutation 3E1 (T888E); 3E2 contains mutations F881E and T888E; 3E2T contains mutations F881E and V894E; 3E2V contains mutations F881E, T888V, and V894E; 3E3 contains mutations F881E, T888E, and V894E; T888V contains mutation T888V; 3E2T contains mutations F881E and V894E; deletion is the mutant with the residues from Ala-880 to Val-894 removed.

for 2 h. The surface CaSR-bound biotin was cleaved with glutathione for 20 min at 4 °C. The cells were then lysed and immunoprecipitated with anti-FLAG M2 antibody and protein A-agarose. Samples were denatured in 2× sample loading buffer and subjected to SDS-PAGE. Biotinylated CaSRs were visualized using the Vectastain ABC immunoperoxidase reagent (Vector Laboratories, Burlingame, CA).

RESULTS

Prediction of a CaM-binding Domain (CaMBD) in the C Terminus of CaSR—The common features of the known CaM-binding regions include net positive charge, high hydrophobicity, and high potential to form an amphipathic helical structure. A CaM-binding site in the C-terminal region of CaSR was predicted by the calmodulin target data base (17). The region with the highest score was located between amino acids Phe-881 and Val-894 (⁸⁸¹FKVAARATLRRSNV⁸⁹⁴) (Fig. 1). There are several known CaM-binding motifs that have been determined based on the spacing of conserved anchoring hydrophobic residues,

such as the 1–14 and 1–10 binding motifs. The putative CaM-binding region in CaSR exhibits a 1–14 binding motif (Fig. 1), which has also been reported in other CaM-binding proteins, such as calcineurin, Na/Ca exchanger, IP₃ receptor, and ryanodine receptor (17). The putative CaM-binding region of CaSR shows a strong propensity to form α -helix based on the secondary structure prediction. Furthermore, helical wheel analysis of the predicted CaM-binding region in CaSR shows that most of the positively charged residues segregate on one side, whereas the hydrophobic residues are located on the other (supplemental Fig. S1), which is similar to the CaM-binding regions in other proteins, such as myosin light chain kinases. It is interesting to note that this predicted CaM-binding region in CaSR aligns well with the known CaM-binding region in mGluR7a (Fig. 1).

CaSR Directly Interacts with CaM in a Ca²⁺-dependent Manner via the Predicted CaMBD—The interaction between CaM and CaSR was confirmed by binary pulldown assays in combination with site-directed mutagenesis studies. First, to examine whether CaM interacts with CaSR, coimmunoprecipitation and CaM-agarose pulldown assays were carried out using lysates from HEK293 cells transfected with CaSR and several receptor constructs mutated in the CaM-binding region. As shown in Fig. 2a, under Ca²⁺-saturated condition, CaM co-immunoprecipitated with the FLAG-tagged CaSR (22) from CaSR-transfected HEK293 cell lysates utilizing an anti-FLAG monoclonal antibody, which suggests that endogenous cellular CaM interacts with CaSR. In contrast, CaM failed to co-immunoprecipitate CaSR when the predicted CaMBD was deleted, regardless of the presence of Ca²⁺. Additionally, CaSR heterologously expressed in HEK293 cells was only pulled down by CaM-agarose in the presence of Ca²⁺ but not in its absence. Because the predicted CaM-binding region exhibits a 1–14-like motif, site-directed mutagenesis at positions 1, 8, and 14 and deletion of this region were performed to confirm the interaction mode between CaM and this predicted CaM-binding region in CaSR (Fig. 1). As shown in Fig. 2b, the Ca²⁺-dependent interaction between CaM and CaSR was partly or completely disrupted after introducing single or multiple mutations at positions 1, 8, and/or 14 (T888E (referred to as 3E1), F881E/V894E (3E2T), F881E/T888V/V894E (3E2V), and F881E/T888E/V894E (3E3)) as well as deleting the predicted CaM-binding region in CaSR (⁸⁸⁰AFKVAARATLRRSNV⁸⁹⁴). On the contrary, substitution of Thr-888 with the more hydrophobic valine (T888V) resulted in an enhanced interaction. Thr-888 is a known PKC phosphorylation site within the C-tail of the CaSR. 3E1 is a pseudophosphorylated analog of this site, whereas T888V cannot be phosphorylated. Thus the impaired and enhanced binding of T888E and T888V, respectively, to the CaSR CaMBD suggests that the capacity of PKC to phosphorylate Thr-888 could be an important regulator of CaM binding to the CaSR and, in turn of signaling by the receptor, as is shown to be the case below.

After confirming the absolute requirement of the predicted CaMBD for the CaM-CaSR association, we next carried out a binary pulldown assay to determine whether the interaction is direct or indirect by using bacterially expressed GST fusion protein and CaM. The predicted CaM-binding domain (residues 868–901) in CaSR was fused to GST with a triple glycine,

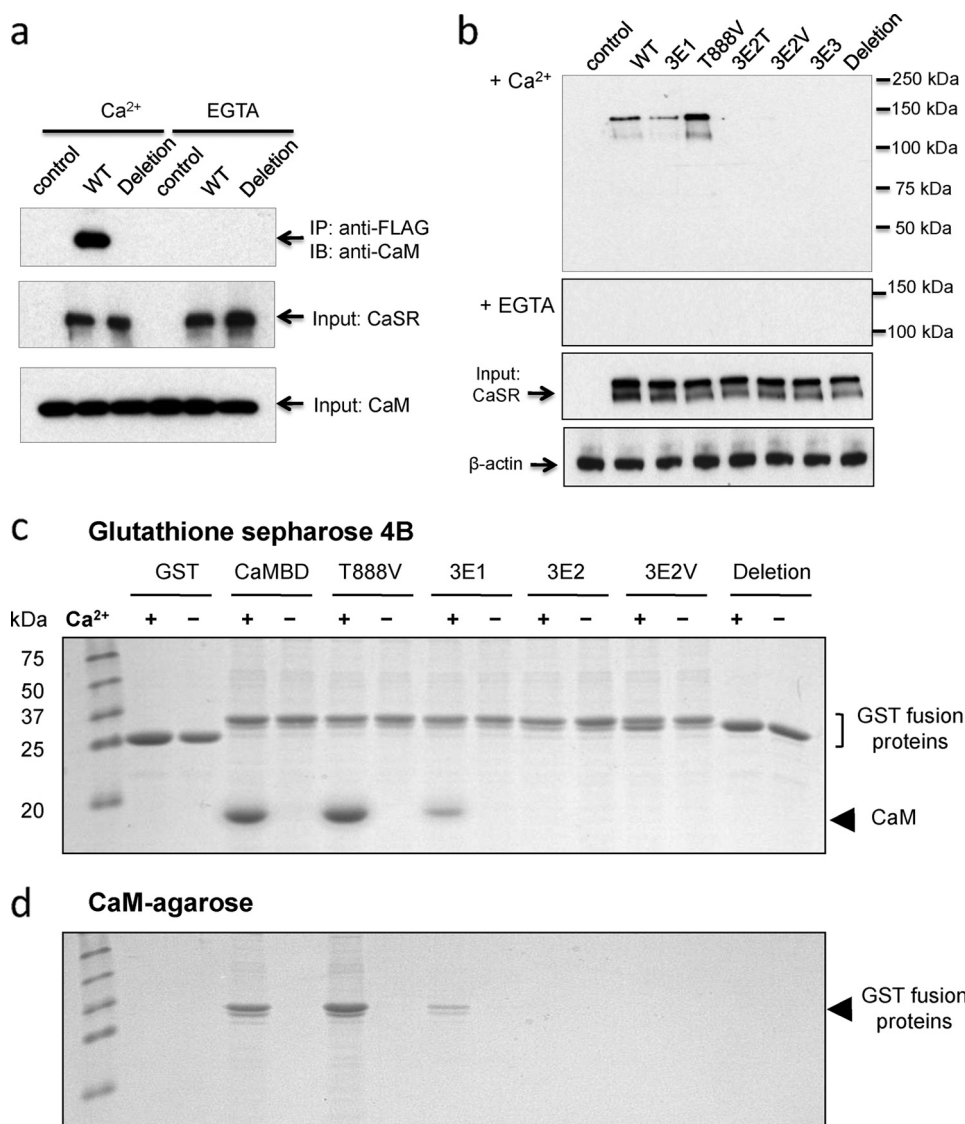


FIGURE 2. Ca²⁺-dependent direct interaction between CaSR and CaM revealed by coimmunoprecipitation and pulldown assays. *a*, Ca²⁺-CaM (but not apo-CaM) co-immunoprecipitated (IP) with CaSR in lysates from the FLAG-tagged CaSR or the deletion mutant-transfected HEK293 cells utilizing an anti-FLAG antibody, suggesting that endogenous cellular CaM interacts with the CaSR. The input CaM and CaSR levels in the total cell lysates were also shown. *b*, CaM-agarose pulldown assay. The cell lysates (0.5 mg of total protein) from HEK293 cells transfected with WT or mutant CaSR were incubated with CaM-agarose beads. The immunoreactions were detected by Western blotting using a monoclonal anti-FLAG antibody. *c*, binding of CaM to GS4B-Sepharose pre-bound with GST or GST fusion proteins under Ca²⁺-loaded (+) and Ca²⁺-depleted (−) conditions. Purified CaM (0.2 mg) was incubated with GS4B-Sepharose with immobilized GST or GST fusion proteins and then resolved by SDS-PAGE after extensive washing. *d*, binding of GST fusion proteins to CaM-Sepharose. GST or GST fusion proteins (0.2 mg) with the predicted WT or mutant CaMBD were incubated with CaM-Sepharose beads and then resolved by SDS-PAGE after extensive washing.

flexible linker (GST-CaMBD). Similarly, mutants containing the mutations T888V, T888E (3E1), F881E/T888E (3E2), F881E/T888V/V894E (3E2V), and the Ala-880 to Val-894 deletion (denoted as deletion) were prepared and fused with GST. Because 3E2V cannot be phosphorylated at Thr-888 and T888V shows enhanced CaM binding, the result with 3E2V documents that it is mutation of the 1 and 14 residues of the CaM-binding site that causes impaired binding of this mutant, and not mutation of the residue at position 8. For the GST pulldown assay, the purified GST-CaMBD or its mutants were immobilized on glutathione-Sepharose 4B and used to prey soluble CaM. As shown in Fig. 2c, Ca²⁺/CaM, but not apo-CaM,

bound to glutathione-Sepharose 4B beads preincubated with GST-CaMBD. A Thr to Val substitution at the predicted anchoring position 8 (residue 888) did not significantly alter the interaction. However, a Thr to Glu substitution (3E1) at this position led to over 50% loss of bound Ca²⁺/CaM. As noted above, this result confirms that pseudophosphorylation of Thr-888 substantially impairs the binding of CaM. The introduction of multiple mutations at predicted anchoring positions (*i.e.* 3E2 and 3E2V) or deletion of the predicted CaMBD, as well as GST by itself, produced mutant GST-CaMBDs that were unable to interact with CaM under both Ca²⁺-loaded and Ca²⁺-depleted conditions. For the CaM-agarose binding assay, CaM-agarose resin was used to pull down the purified GST fusion proteins (Fig. 2d). WT GST-CaMBD and the mutant T888V only bound to CaM-agarose resin in the presence of Ca²⁺, whereas the pseudophosphorylated mutant, 3E1, was much less efficient in interacting with CaM resin. Again, 3E2, 3E2V, the deletion mutant, and GST itself failed to interact with CaM resin regardless of the presence or absence of Ca²⁺. Overall, these studies clearly establish a Ca²⁺-dependent, direct association between CaM and the predicted CaMBD in CaSR with high specificity and demonstrate that the state of phosphorylation of Thr-888 is an important modulator of CaM binding.

Structural Changes during CaM-Target Complex Formation and Determination of Binding Stoichiometry—We then resorted to

spectroscopic techniques to probe structural changes accompanying formation of the CaM-CaMBD complex. Peptide models have been very useful in probing the role of CaM in regulating many biological processes, such as Ca²⁺-mediated inhibition of gap junctions (21, 23). To perform detailed structural studies, a peptide fragment was synthesized corresponding to the predicted CaM-binding region in CaSR (residues 871–898). We first examined the secondary structural changes upon complex formation using circular dichroism spectroscopy. As shown in Fig. 3a, the addition of the peptide to Ca²⁺/CaM led to signals that were 20% more negative between 205 and 235 nm. In the absence of Ca²⁺, no

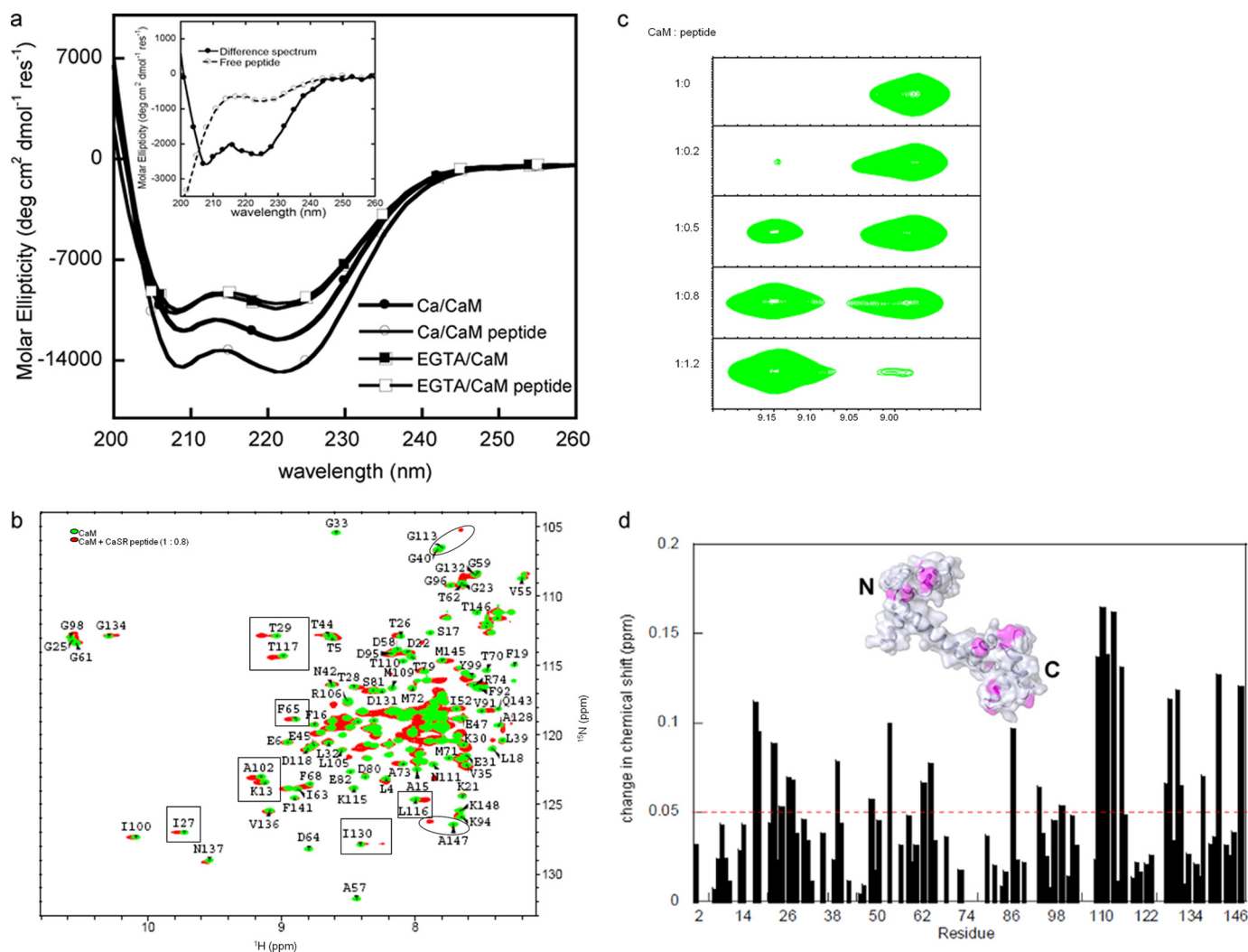


FIGURE 3. Biophysical characterization of the interaction between Ca²⁺/CaM and the CaMBD peptide derived from CaSR. *a*, the far-UV circular dichroism (CD) spectra of 10 μ M Ca²⁺/CaM and apo-CaM with or without the addition of the peptide. *Inset*, the far-UV CD spectra of the peptide (*dashed line*) and the calculated difference spectrum (*solid line*) obtained by subtracting the spectrum of Ca²⁺/CaM from that of the Ca²⁺/CaM-peptide complex. *b*, detection of Ca²⁺/CaM-peptide interaction using two-dimensional NMR. Overlay of the ¹H-¹⁵N-HSQC spectrum of CaM (0.3 mM) with the spectrum of the CaM-peptide complex in the presence of 5 mM Ca²⁺. The boxed regions show residues undergoing obvious chemical shift movements. *c*, the chemical shift change of residue Thr-29 as a function of the CaM/peptide molar ratio. *d*, histogram of residue-specific chemical shift changes after binding of the peptide to Ca²⁺/CaM. Residues exhibiting changes of over 0.1 ppm are highlighted in magenta on the three-dimensional structure of Ca²⁺/CaM (PDB entry 3CLN). *e*, correlation between experimentally measured ¹H-¹⁵N RDCs of the Ca²⁺/CaM-CaSR complex and the best-fit RDC values calculated with the CaM-eNOS structure (PDB entry 1NIW). *f*, ITC studies on the interaction between Ca²⁺/CaM and the CaMBD peptide derived from CaSR. *Left*, representative trace of the calorimetric titration of the peptide (20 μ M) with CaM (400 μ M) in 20 mM HEPES, 150 mM KCl, 1 mM CaCl₂ (pH 7.5) at 25 °C. *Right*, comparison of enthalpic (ΔH , red) and entropic ($-\Delta S$, blue) contributions to the Gibbs free energy (ΔG , black) of Ca²⁺-CaM/peptide complexes adopting a global wrapping around the 1–14 mode of interaction (*, data were obtained from Ref. 43).

significant difference was observed before or after addition of the peptide, which is consistent with the results of the CaM-agarose pulldown assay and further confirms a Ca²⁺-dependent association between CaM and the CaMBD in CaSR. The difference spectrum (Fig. 3*a*, *inset*) clearly shows two troughs, one at 208 nm and the other at 222 nm, indicating the formation of a more helical structure upon complex formation. The net increase in the CD signal is attributable to a higher degree of α -helicity in the peptide, because the helical content of CaM does not increase significantly (<2%) upon complex formation. This observation agrees with our prediction of a helical conformation of the CaM-binding region in the CaSR (Fig. 1). In addition, the peptide adopted a typical helical conformation in the presence of

trifluoroethanol, a helix stabilizing solvent (supplemental Fig. S2). All these results support the conclusion that the predicted CaM-binding region in CaSR possesses a strong propensity to form α -helix, which is one of the essential properties of most known CaMBDs.

Because the chemical shifts of protein amides are very sensitive to even subtle conformational changes occurring at the interacting interface, chemical shift perturbations can be used to identify the interaction surface following complex formation. Therefore, we examined the peptide-induced structural changes in CaM by monitoring the chemical shift changes of the CaM backbone amides with ¹H-¹⁵N-HSQC spectroscopy. Titration was carried out by adding unlabeled peptide to ¹⁵N-labeled CaM. As shown in Fig. 3*b*, the HSQC spectrum of Ca²⁺/

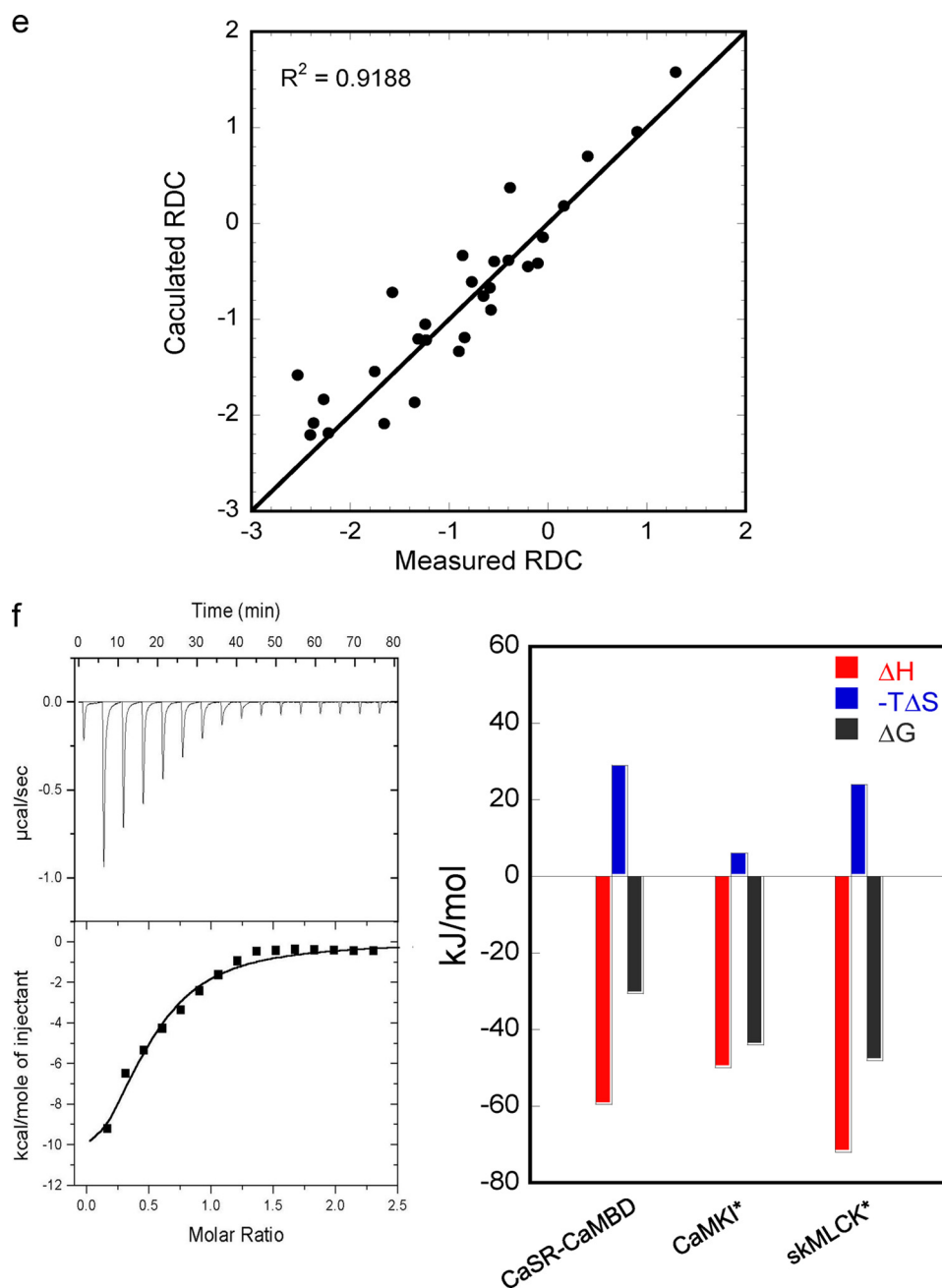


FIGURE 3—continued

CaM is almost identical to the previously described spectra (23), allowing us to unambiguously assign a number of dispersed peaks. The addition of the peptide to CaM led to global chemical shift perturbations that involved both the N-domain (e.g. Ser-17, Thr-29, Gly-33, Asn-53, Ala-57, and Asp-64) and the C-domain (e.g. Met-109, Thr-115, Asn-111, Gly-113, Ala-128, Ile-130, Phe-141, and Ala-147) of CaM, implying global conformational changes associated with this interaction. The detailed chemical shift change for each residue is shown in Fig. 3*d*. During the titration, a progressive disappearance of the amide signals of the unbound CaM was accompanied by the concomitant emergence of a new set of peaks arising from the peptide-bound CaM (Fig. 3*c*), indicating a slow exchange process in which the exchange rate of

the bound and unbound states is smaller than the amide frequency difference between the two states. Such phenomena have been observed previously following protein-protein or protein-peptide associations (24) with affinities at micromolar or submicromolar ranges. As shown in Fig. 3*c*, the peak at 9.03 ppm was diminished at a 1:1 ratio, whereas at 9.15 ppm it reached a maximum, suggesting a 1:1 complex formation.

RDC has been used to assist in homology modeling, determine relative domain orientations in multidomain proteins, and characterize molecular binding processes (25, 26). This recently developed technique has been applied to investigate the complex mode of calmodulin and its target peptide/fragments (26, 27). To assess the binding mode of CaM and the CaSR utilizing this approach, we compared the measured RDCs with calculated values from structures deposited in the Protein Data Bank (PDB) (listed in [supplemental Table S1](#)). We selected structures in which CaM binds by wrapping around the peptide using both its N- and C-terminal domains (PDB codes 2HQW, 1CDM, 1NIW, 1IQ5, and 2BCX), as well as by binding in an extended conformation (PDB codes 2IX7, 1CFF, 1K93, 1NWD, and 1G4Y). We also compared the data with the structure of the CaM by itself (PDB code 3CLN). The quality of the fit is determined by the Q-factor, as well as the agreement between domain orientations. For a globular protein complex, it is expected that only

small domain rotations in Euler angles are required to obtain co-linearity of the alignment tensors (19). As shown in Fig. 3*e* and [supplemental Table S1](#), the best correlations of measured and calculated RDCs (low Q-factor) were observed when the RDCs were fitted using the structure of the CaM-eNOS (endothelial nitric-oxide synthase) complex (PDB entry 1NIW) (28) with a 1–14 binding mode. These results are consistent with our results from chemical shift analysis and mutagenesis studies.

To resolve the origin of the energetic changes underlying the interaction between CaM and the synthetic peptide, ITC studies were performed at 25 °C (Fig. 3*f*). Similar to the thermodynamics of other well studied CaM-peptide complexes (such as CaM-dependent kinase I (29) and skeletal muscle myosin light

chain kinase (30) that adopt a “wrapping around” 1–14 mode of interaction, the binding event was found to be exothermic, enthalpically favorable ($\Delta H = -59.5 \pm 5.6 \text{ kJ mol}^{-1}$), but entropically unfavorable ($\Delta S = -96.9 \pm 18.1 \text{ J mol}^{-1}$), with an association constant of $K_a = 2.2 \pm 0.2 \times 10^5$ (or $K_d = 4.6 \pm 0.5 \text{ }\mu\text{M}$) and a stoichiometry of 0.9 ± 0.1 . Overall, the combined chemical shift perturbation, RDC, and ITC analyses provide compelling evidence of a wrapping-around binding mode of the Ca²⁺/CaM-CaSR complex with 1–14 binding mode.

Determination of the Binding Constant of CaM to CaSR—Quantitative determination of the binding of CaM to the CaMBD in CaSR was achieved using dansylated CaM by monitoring changes of dansyl fluorescence emission as well as anisotropy changes. As shown in Fig. 4*a*, upon the addition of GST-CaMBD, the fluorescence signal of dansyl-CaM increased by 1.2-fold, and the fluorescence emission peak was blue-shifted from 495 to 489 nm in the presence of Ca²⁺. These data indicate that the dansyl group in CaM undergoes a conformational change and enters a more hydrophobic environment after complex formation. Such changes were not observed after adding GST or after adding GST-CaMBD in the presence of EGTA. Fluorescence anisotropy measurements were carried out to further confirm the binding event (Table 1). The anisotropy for Ca²⁺/dansyl-CaM alone was found to be 0.038. On addition of GST-CaMBD, the anisotropy increased to 0.092, strongly indicating a slower tumbling of the fluorophore due to the formation of a larger complex. Addition of one of the mutant proteins, GST-CaMBD-3E1, led to a modest increase in anisotropy from 0.038 to 0.068. In contrast, addition of the deletion mutant did not change the anisotropy at all. Furthermore, no significant changes in anisotropy were detected before or after addition of GST or GST fusion proteins under Ca²⁺-depleted conditions, which is in good agreement with the steady-state fluorescence measurements.

The significant enhancement of the dansyl fluorescence signals allowed us to further determine the dissociation constants of CaM for its binding to the predicted CaMBD as well as to its various mutant forms. As shown in Fig. 4*c* the titration data were well fitted with a 1:1 stoichiometry with the observed K_d values listed in Table 2. The dissociation constant of GST-CaMBD for dansyl-CaM was determined to be $0.3 \pm 0.1 \text{ }\mu\text{M}$. The binding affinity of the mutant 3E1 (T888E) was found to be at least 21-fold weaker ($6.3 \pm 0.1 \text{ }\mu\text{M}$). After the introduction of one (F881E/T888E, 3E2) or two (F881E/T888E/V894E, 3E3) additional mutations in the proposed anchoring positions, the predicted CaMBD failed to associate with dansyl-CaM at all. All these results were consistent with the binary pulldown data described above.

Loss of the CaM-binding Domain in CaSR Perturbs [Ca²⁺]_o-induced [Ca²⁺]_i Signaling—To test whether CaM binding to the predicted CaM-binding region in the CaSR has an important role in transducing extracellular Ca²⁺ signals into intracellular Ca²⁺ signaling, we measured changes in [Ca²⁺]_i and associated [Ca²⁺]_o oscillations in response to elevations in [Ca²⁺]_o in HEK293 cells transfected with WT CaSR or its mutants. First, we examined the cellular localization of CaSR and its mutants after transfection and expression. As expected, all WT

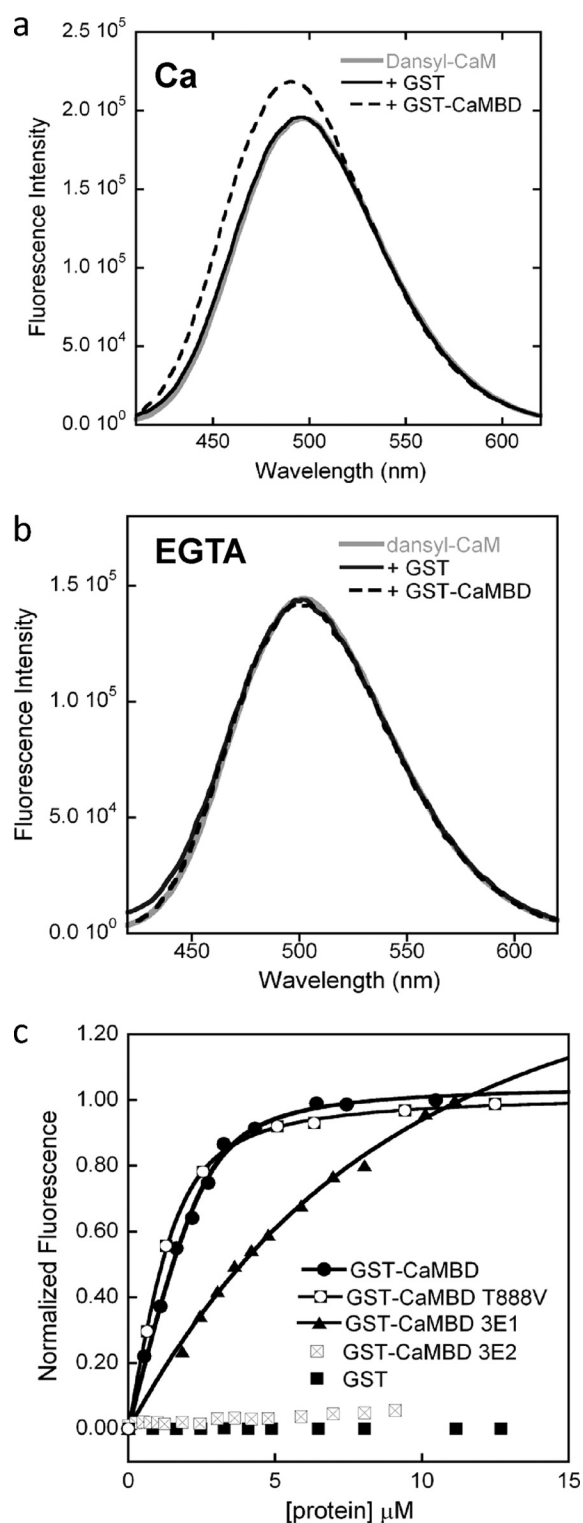


FIGURE 4. Detection of Ca²⁺-dependent specific interaction between dansyl-CaM and the predicted CaMBD (as GST fusion protein) by fluorescence spectroscopy. *a* and *b*, dansyl fluorescence spectra of dansyl-CaM (3 μM), dansyl-CaM:GST (1:2) mixture, and dansyl-CaM:GST-CaMBD (1:2) mixture in the presence of Ca²⁺ (*a*) or EGTA (*b*). *c*, plot of the relative fluorescence intensity changes as a function of GST or GST fusion proteins. The titration curve is fitted as a 1:1 binding process.

and mutant CaSRs were expressed on the plasma membrane, with some variation in the level of cell surface expression (supplemental Figs. S3 and S5). Next, the intracellular Ca²⁺ level

TABLE 1

Fluorescence anisotropy of dansyl-CaM (3 μ M) with and without GST fusion proteins ($n = 3$)

Sample	Anisotropy	
	+EGTA	+Ca ²⁺
Dansyl-CaM	0.026 \pm 0.005	0.038 \pm 0.005
Dansyl-CaM + GST (1:2)	0.027 \pm 0.008	0.039 \pm 0.008
Dansyl-CaM + GST-CaMBD (1:2)	0.026 \pm 0.009	0.092 \pm 0.007 ^a
Dansyl-CaM + GST-CaMBD del (1:2)	0.026 \pm 0.004	0.038 \pm 0.004 ^a
Dansyl-CaM + GST-CaMBD 3E1 (1:2)	0.026 \pm 0.004	0.068 \pm 0.004

^a $p < 0.01$.

TABLE 2

Binding constants of GST fusion proteins for dansyl-CaM in the presence of Ca²⁺ ($n = 3$)

Sample	K_d^a
	μ M
GST-CaMBD	0.3 \pm 0.1
GST-CaMBD T888V	0.3 \pm 0.1
GST-CaMBD deletion	ND ^b
GST-CaMBD 3E1	6.3 \pm 0.1
GST-CaMBD 3E2	ND
GST-CaMBD 3E3	ND

^a Data were obtained by fitting the titration curves shown in Fig. 4c as 1:1 binding processes.

^b ND, not detectable due to weak interactions.

was monitored while increasing [Ca²⁺]_o. The EC₅₀ values and maximal responses were normalized based on the relative levels of cell surface expression of the CaSR and its mutants. As shown in Fig. 5a and listed in Table 3, substitutions in the predicted CaM-binding residues of CaSR at positions 1, 8, and 14 led to right shifting of the [Ca²⁺]_i response curves to elevations of [Ca²⁺]_o, resulting in substantial increases in the EC₅₀ values for [Ca²⁺]_o. Furthermore, the maximal responses of the mutant receptors decreased to ~72–94%, defining the response of WT CaSR as 100%. Because mutant 3E2T disrupts two of the three CaM anchoring residues whereas leaving the PKC site Thr-888 intact, it removes the confounding effect of mutating residues that are both a PKC site and a CaM anchoring residue (e.g. as in 3E1 or 3E2). Meanwhile, the maximal response of T888V, a mutant with a hydrophobic valine that removes the PKC site at this residue and enhances the interaction between CaSR and CaM, increased to 140%. More strikingly, the deletion mutant exhibited almost no response toward extracellular Ca²⁺ changes. Given that the mutants 3E2 and 3E3, which similarly failed to interact with CaM, still preserve reduced Ca²⁺ responses, it is likely that deletion of this region has adverse effects on the structural integrity and functionality of other regions of the cytoplasmic tail of CaSR, which also contribute to the Ca²⁺ response.

It has been reported that increases of extracellular Ca²⁺ to 2–3 mM can induce intracellular Ca²⁺ oscillations in HEK293 cells expressing CaSR (31–33). We then examined the [Ca²⁺]_i oscillatory frequencies in HEK293 cells transfected with CaSR and its mutants. The frequency of [Ca²⁺]_i oscillations was altered in cells transfected with CaSR mutants relative to WT CaSR. Fig. 5b shows the typical oscillation patterns of HEK293 cells transfected with wild type or mutant CaSRs. The frequency of [Ca²⁺]_i oscillations in HEK293 cells transfected with wild type CaSR was found to be ~2/min, which is comparable with the value reported in other studies (32, 33). Interestingly, for HEK293 cells transfected with mutants 3E1 (T888E), 3E2

(F881E/T888E), 3E3 (F881E/T888E/V894E), 3E2T (F881E/V894E), all of which disrupt interaction with CaM, or T888V, which eliminates the PKC phosphorylation site but retained binding to CaM, the oscillation frequencies, were reduced to 1.2, 0.8, 0.5, 1.3, and 0.6/min, respectively. Most cells transfected with mutant CaSRs underwent oscillation when [Ca²⁺]_o was increased to 5 mM. The oscillation patterns were particularly altered in cells expressing 3E1 (T888E). The intracellular Ca²⁺ signals in cells transfected with 3E1 (T888E) first underwent oscillations and then exhibited sustained responses. In addition, 3E2 and 3E3, which have markedly reduced CaM binding and exhibited the greatest reductions in oscillation frequency, also have the highest EC₅₀ values of their intracellular calcium responses. Moreover, addition of the CaM antagonist, W7, an inhibitor mainly blocking Ca²⁺/CaM-activated phosphodiesterase, myosin light chain kinase, and other CaM-dependent processes, led to the total disappearance of Ca²⁺ oscillations in HEK293 cells transfected with either WT or mutant CaSRs, although a substantial sustained response to [Ca²⁺]_o persisted (Fig. 5c). In addition, we investigated whether mutations in the predicted CaMBD affect the cAMP signaling pathway. Results of these studies indicated that CaSR mutants 3E1 (T888E) and 3E3 (F881E/T888E/V894E) have no effects on the cAMP signaling pathway (supplemental Fig. S4).

CaM Dynamically Regulates the Trafficking of CaSR—To further understand the role of CaM binding in CaSR-mediated [Ca²⁺]_i signaling, we next monitored cell surface expression and internalization of the receptor using a biotin protection assay and a dual fluorescence-based antibody uptake internalization assay under non-permeabilizing conditions. First, CaSR-transfected HEK293 cells were labeled with disulfide-cleavable biotin, incubated in calcium-free buffer for 40 min, and then stimulated with 4 mM Ca²⁺ for 2 h (34). The internalized biotin-labeled CaSR was protected from disulfide cleavage, whereas biotin-labeled CaSR remaining on the surface was cleaved. The biotin-labeled CaSR was immunoprecipitated with the anti-CaSR antibody and revealed by streptavidin peroxidase (see supplemental “Methods” for details). As shown in Fig. 6a, over two-thirds of the wild type CaSR remained on the cell surface, with ~30% of the receptor internalized. In contrast, internalization was significantly increased for 3E3 and the deletion mutant (with three of the predicted CaM anchoring residues substituted or the CaMBD removed entirely, respectively), whereas the total protein level of CaSR expression appeared to be unchanged.

Surface expression of the CaSR was then detected using anti-CaSR antibody staining of non-permeabilized cells followed by confocal fluorescence microscopy. Fig. 6b shows that the WT CaSR and its variants were expressed on the plasma membrane at both 1 and 4 mM [Ca²⁺]_o. However, because of cell-to-cell variation, it was difficult to quantitate the relative levels of CaSR expression among the various CaSRs tested. Intracellular CaSR was revealed by permeabilizing the cells and using an anti-CaSR antibody conjugated with a different fluorophore in cells in which cell surface CaSR had already been labeled with the first antibody. Consistent with the results of the biotin protection assay, CaSR variants with CaM anchoring residues mutated, such as 3E2T, 3E2V, and 3E3, exhibited significant

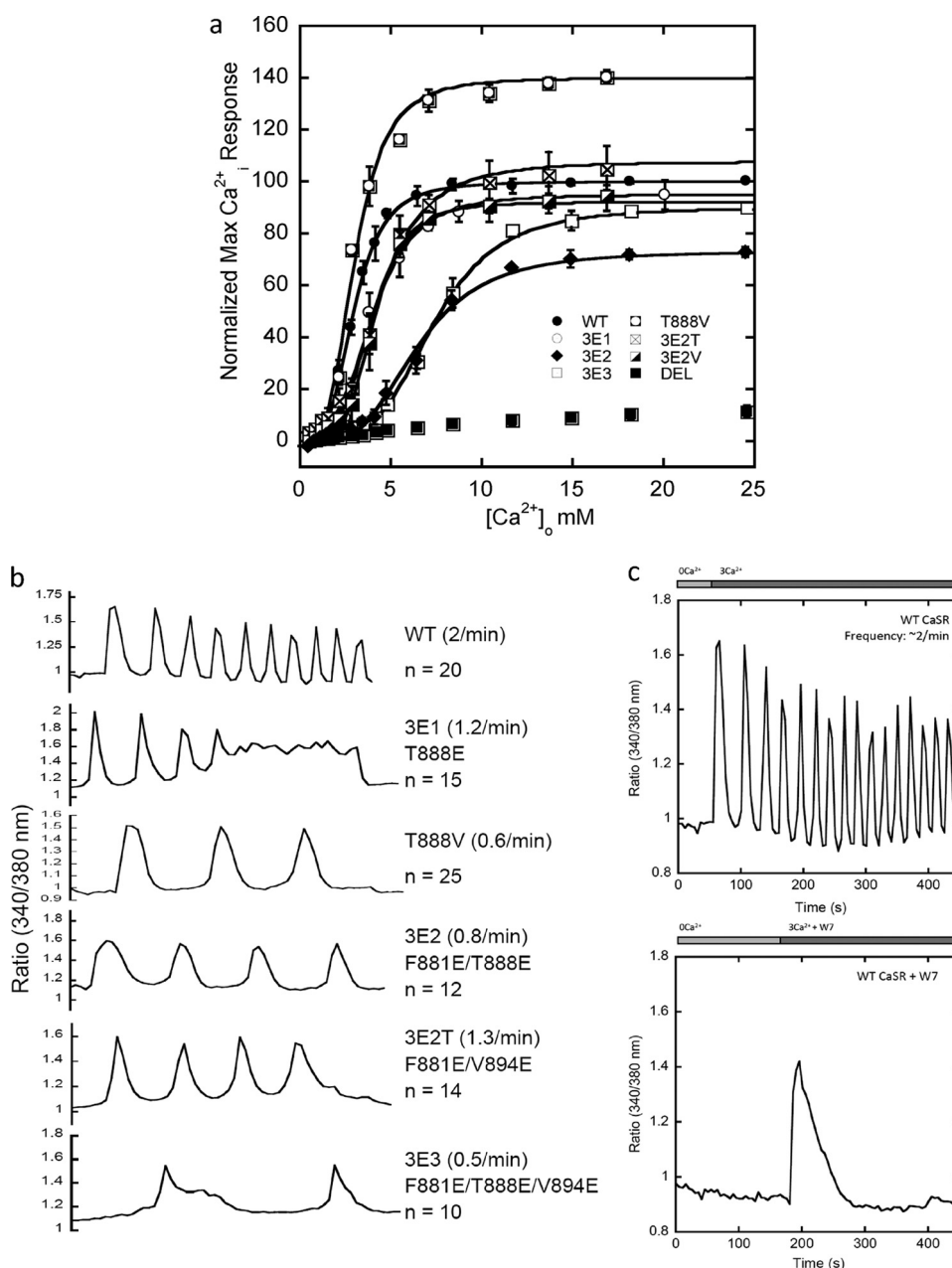


FIGURE 5. Effects of CaMBD mutations on [Ca²⁺]_o-evoked intracellular Ca²⁺ responses. *a*, effects of mutations in the predicted CaMBD of the CaSR were assayed by monitoring intracellular Ca²⁺ signals (using Fura-2) in response to stepwise changes in [Ca²⁺]_o. Functional characterization of the WT CaSR and CaSRs with mutations was performed using HEK293 cells transiently transfected with the WT or mutant CaSR. The surface expression levels of WT and mutant receptors were determined using FACS by taking advantage of a FLAG epitope inserted within the ECD region of CaSR (supplemental Fig. S5). The intracellular calcium response curves were normalized to the expression levels of the respective receptors. *b*, [Ca²⁺]_i oscillation frequency of HEK293 cells expressing CaSR and the mutants. The intracellular Ca²⁺ oscillations induced by elevation of [Ca²⁺]_o mediated by wild type CaSR and its mutants. HEK293 cells were transfected with wild type CaSR or its mutants, 3E1 (T888E), T888V, 3E2 (F881E/T888E), and 3E2T (F881E/V894E), and the intracellular Ca²⁺ oscillations were measured by monitoring the fluorescence signals of Fura-2-loaded HEK293 cells. *c*, [Ca²⁺]_i oscillations in HEK293 cells transfected with CaSR in the absence or presence of the calmodulin agonist W7 monitored using Fura-2 AM.

increases in the amount of intracellular receptor in the presence of high Ca²⁺ (4 mM) (note the increases in regions of diffuse and dense intracellular staining at 4 mM [Ca²⁺]_o with 3E2T, 3E2V, 3E3, and deletion). These results suggest that the CaM-binding region of the CaSR is important for maintaining surface expression of the receptor.

In addition to monitoring internalization at the single-cell level using confocal microscopy, we further set out to quantitate and compare statistically the internalization levels among WT and mutant CaSR receptors using fluorescence-activated cell sorting (FACS). A similar protocol was used as in the dual-color CaSR internalization assay. Surface FLAG-tagged CaSR was detected with a monoclonal anti-FLAG antibody and then quantitated using Alexa Fluor 488-conjugated, goat anti-mouse IgG under non-permeabilizing conditions, whereas internalized CaSR was subsequently determined by using Cy5-conjugated, goat anti-mouse IgG under permeabilizing conditions. The percentage of internalized CaSR was calculated using fluorescence intensity from Cy5 divided by the total fluorescence intensity (relative signals from Cy5 and Alexa Fluor 488 combined). As shown in Fig. 6c, the internalization levels of 3E3 and the deletion mutant were significantly increased at 4 mM Ca²⁺, which confirmed the results at the single cell level.

DISCUSSION

In the present study, we have characterized how CaM interacts with the C-tail of CaSR, a member of the family C GPCRs responsible for sensing extracellular Ca²⁺ levels, maintaining extracellular Ca²⁺ homeostasis, and transducing calcium signaling from extracellular to intracellular environments. We have demonstrated a Ca²⁺-dependent stoichiometric interaction between the C-tail of CaSR and CaM. Such an interaction appears to be critical for maintaining a proper intracellular Ca²⁺ response to changes in extracellular Ca²⁺, in terms of the magnitude of the response, EC₅₀ for [Ca²⁺]_o, and oscillation frequency.

The data reported herein indicate that binding of CaM induced significant changes in the secondary and tertiary structures of a peptide derived from the predicted CaMBD of CaSR. Following the formation of the CaM-peptide complex in the presence of Ca²⁺, a more helical structure is detected in the peptide. Analysis of the amino acid sequence indicates that

TABLE 3**Intracellular Ca²⁺ responses of wild type CaSR and its CaMBD mutants (n = 3)**

Mutations	Maximal response	Ca ²⁺ , EC ₅₀	n _{Hill}
	%	mM	
WT	100	3.0 ± 0.1	3.6 ± 0.1
T888V	140 ± 3 ^a	3.0 ± 0.1	3.3 ± 0.2
3E1	94 ± 1	4.0 ± 0.1 ^b	3.7 ± 0.2
3E2T	78 ± 8 ^b	4.2 ± 0.1 ^a	3.6 ± 0.4
3E2V	95 ± 3	4.0 ± 0.4 ^b	4.5 ± 0.6
3E2	59 ± 3 ^a	6.8 ± 0.6 ^a	3.4 ± 0.3
3E3	72 ± 3 ^b	7.2 ± 0.3 ^a	4.1 ± 0.3
Deletion	11 ± 3 ^a	NA ^c	NA
WT + W7	145 ± 7	3.2 ± 0.2	2.7 ± 0.5

^a p < 0.01.^b p < 0.05.^c NA, not available.

interaction between CaM and the CaSR C-tail falls into the 1–14 class binding mode, which is similar to the well characterized, 1–14 CaM-binding motifs in mGluR7a or eNOS (28). This conclusion is further corroborated by residual dipolar coupling NMR studies. In addition, the binding event is mostly enthalpically driven with unfavorable changes in entropy, much like the thermodynamic scenario visualized in other CaM-target peptide complexes that undergo global conformational changes with anchoring residues located at positions 1 and 14, such as CaM-dependent kinase I (29) and skeletal muscle myosin light chain kinase (30). NMR chemical shift perturbation data clearly demonstrate that both domains of CaM undergo structural changes upon binding of the peptide. Peptide binding leads to extensive structural rearrangement in CaM, most likely because of the embracing mode of interaction that has been thus far most commonly reported, as best exemplified by myosin light chain kinases and CaM-dependent kinases (35, 36). This binding involves the unwinding of the central linker in CaM, enabling the N- and C-domains of CaM to accommodate the target peptides in a wrap-around fashion. During the titration of the peptide to Ca²⁺/CaM, the chemical shift changes of CaM are characteristic of slow exchange on the NMR time scale. Such an exchange rate implies that the binding affinity of the peptide to holo-CaM is at least at the micromolar or sub-micromolar level. Indeed, the dissociation constant for the predicted CaMBD to CaM was determined to be ~0.3 μM as a GST fusion peptide, and ~5 μM as a synthetic peptide.

The next question we addressed was the physiological correlation and functional relevance of the association of Ca²⁺/CaM with the C-tail of CaSR. CaSR has been shown to transduce external stimuli into activation of intracellular Ca²⁺ signaling cascades via G_{q/11} or to inhibit the cAMP signaling pathway through G_{α_i}. [Supplemental Fig. S4](#) shows that the level of cAMP is comparable among cells transfected with WT CaSR or mutants harboring various mutations in the predicted CaMBD. In addition, elevating [Ca²⁺]_o did not lower cAMP suggesting that there may not be efficient coupling of CaSR to G_{α_i} and adenylate cyclase in the HEK293 cells utilized here.

We next investigated the G_{q/11}-mediated signaling pathway. Several groups have reported that the C-tail of CaSR is critical for [Ca²⁺]_i signal transduction via this pathway. For example, Ray *et al.* (37) demonstrated that mutations of residues F881A/K882A/V883A in CaSR significantly reduced the intracellular Ca²⁺ response to external Ca²⁺. Bai *et al.* (38) reported that

phosphorylation at Thr-888 in CaSR inhibits its coupling to Ca²⁺ store release and Davies *et al.* (31) found that phosphorylation at Thr-888 modulates CaSR-induced [Ca²⁺]_i oscillations. Substitution of Thr-888 with Val in our studies abrogates phosphorylation by PKC and leads to a dramatic decrease in the [Ca²⁺]_i oscillation frequency (from 2 to 0.6/min), although the mechanism underlying this effect is unclear because phosphorylation of this site in an earlier study reduced Ca²⁺_i signaling. However, because the CaM-binding affinity of this mutant and its maximal response to [Ca²⁺]_o were comparable with or greater than those of the wild type receptor, it appears that the overall signaling efficiency of T888V is more closely related to these latter parameters than to its oscillation frequency.

Our results have revealed a new mechanism of CaM-induced modulation of [Ca²⁺]_i signaling by the CaSR. Our studies using site-directed mutations/deletion in the CaM-binding region in the C-tail of CaSR indicate that this region is essential for CaSR-mediated intracellular Ca²⁺ signaling. First of all, this region seems to be important for the maintenance of proper sensitivity of the CaSR-mediated intracellular Ca²⁺ responses to altered [Ca²⁺]_o, as illustrated by the increases in EC₅₀ resulting from mutations of the CaM-binding domain of CaSR. In addition, agonist-induced, sustained intracellular Ca²⁺ oscillations at a frequency similar to those evoked by the wild type CaSR appear to require that this region be intact. Substitution of two of the three proposed CaM-anchoring residues (Phe-881, Thr-888, and/or Val-894) in the CaSR C-tail with glutamates significantly slows the intracellular Ca²⁺ oscillations. Moreover, without changing the residue essential for PKC-mediated phosphorylation (Thr-888), the CaSR variant with mutations at Phe-881 and Val-894 (F881E/V894E mutant, 3E2T) exhibited a substantially slower oscillation frequency (1.3/min compared with 2/min for the wild type CaSR), supporting the importance of CaM binding to the CaSR *per se* for maintenance of a normal [Ca²⁺]_i oscillatory response to an elevated level of [Ca²⁺]_o. This view is further indirectly corroborated by the observation that [Ca²⁺]_i oscillation frequency is disrupted by the CaM inhibitor, W7. In addition to directly perturbing the interaction between CaM and CaSR, W7 might also disrupt other CaM-mediated signaling pathways. However, the greatest increases in EC₅₀ and reductions in oscillation frequencies were observed in mutants in which there are both disruption of the CaM-binding site and pseudophosphorylation of Thr-888 (mutation to Glu in mutants 3E2 and 3E3). This result suggests a synergistic action of phosphorylation of the PKC phosphorylation site and disruption of CaMBD in inhibiting signaling by the CaSR. Thus in the absence of CaM binding, activation of the PKC site further impairs receptor-effector coupling. One possible mechanism underlying this interaction could be that in addition to directly inhibiting Ca²⁺ release from intracellular stores (31) by interfering with signal transduction/receptor trafficking, phosphorylation of Thr-888 also impairs CaM binding, which has a further negative impact on receptor function/trafficking (see below). Indeed, mutation of Thr-888 to Glu-888, which cannot be reversibly phosphorylated/dephosphorylated, reduced CaM binding affinity by about 20-fold. Therefore, PKC phosphorylation of Thr-888 could serve as a “switch” between CaM-mediated effects on the function of receptor when this residue

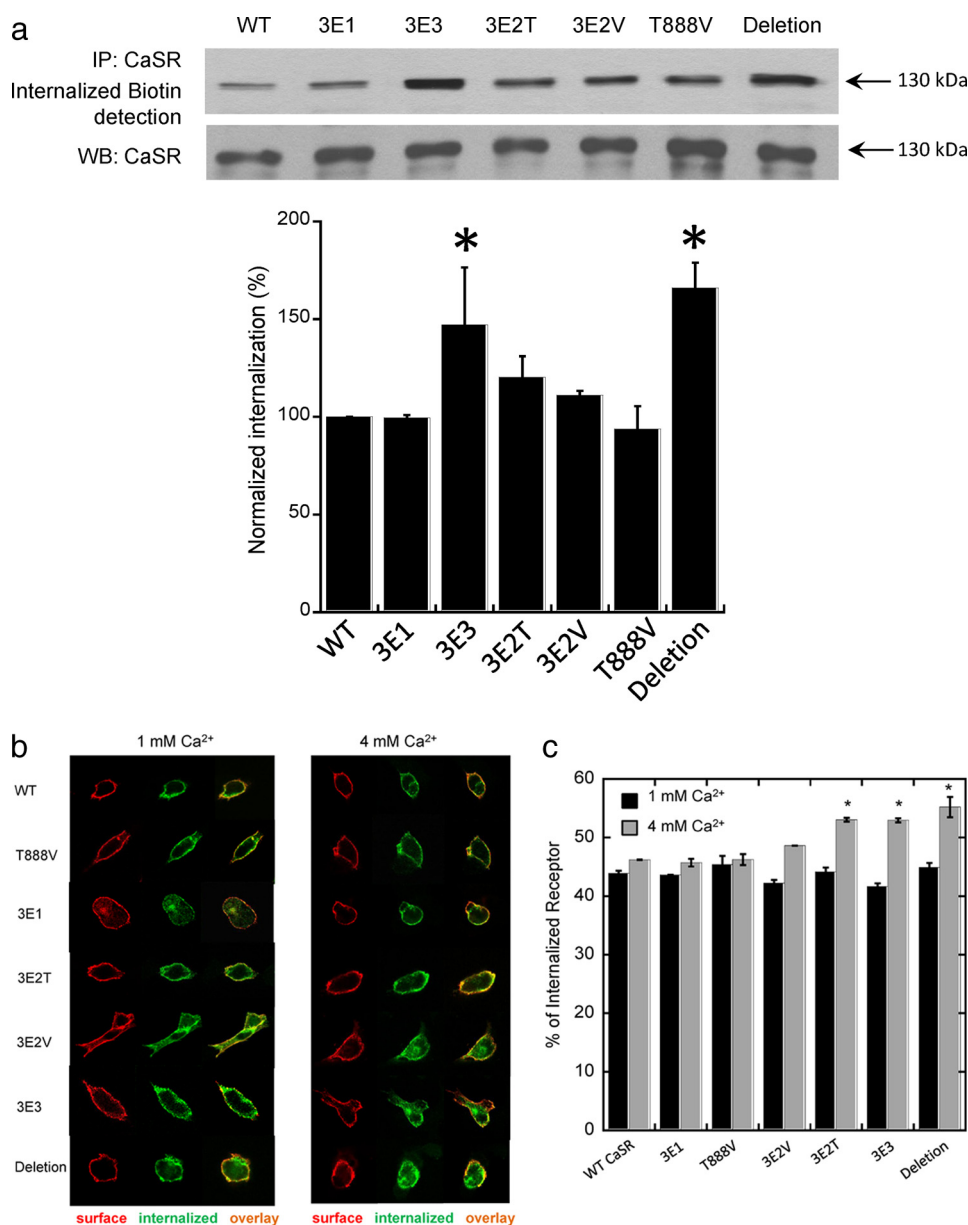


FIGURE 6. Effects of mutations in the predicted CaMBD on cell surface expression and internalization of wild type and mutant CaSR. *a*, quantification of internalized CaSR with the biotin protection assay. CaSR-transfected HEK293 cells were labeled with disulfide-cleavable biotin, incubated in calcium-free buffer for 40 min, and then stimulated with 4 mM Ca²⁺ for 2 h. The internalized CaSR was immunoprecipitated with the anti-FLAG antibody and revealed by streptavidin peroxidase. The intensity in each lane was quantified using ImageJ, and the error bars represent S.E. for two to three independent experiments. *, $p < 0.05$, compared with WT (Student's *t* test). *b*, dual fluorescence-based antibody uptake internalization assay. Surface expression and intracellular CaSR as assessed by CaSR antibody staining of non-permeabilized (red staining) or permeabilized (green staining) cells, respectively, and imaging with confocal fluorescence microscopy. The WT CaSR and its mutants are expressed in the plasma membrane at both 1 and 4 mM [Ca²⁺]_o. Notably, the 3E3 and deletion mutants, unlike the WT CaSR, show significant internalization at 4 mM [Ca²⁺]_o. *c*, quantification of CaSR internalization with FACS. HEK293 cells transfected with wild type CaSR or mutant CaSRs were incubated with anti-FLAG antibody at 4 °C for 1 h and then treated with 1 or 4 mM Ca²⁺ for 2 h, respectively, followed by incubation with Alexa Fluor 488-conjugated, goat anti-mouse IgG for 1 h at 4 °C. Then cells were permeabilized with 1% Triton X-100 and internalized CaSR was stained with Cy5-conjugated anti-mouse IgG. 10⁶ cells were collected and fluorescence intensity was measured using FACS. The percentage of internalized CaSR was calculated using fluorescence intensity from Cy5 divided by the total fluorescence intensity (signals from both Cy5 and Alexa Fluor 488). The error bars represent the S.D. for three independent experiments. *, $p < 0.05$, compared with WT at 4 mM Ca²⁺ (Student's *t* test). WB, Western blot.

is not phosphorylated and PKC-mediated effects when it is (Fig. 7).

Chang *et al.* (39) reported that the amino acids in the cytoplasmic C terminus of the CaSR are important for the cell sur-

face expression of the CaSR. Several proteins, such as receptor activity-modified proteins (40) and Rab11a (34), were shown to regulate the trafficking of the CaSR. Filamin A and the E3-liagase Dorfin were reported to stabilize and promote degradation of the CaSR, respectively (7, 9). Here, we have clearly demonstrated that residues involved in CaM binding within the cytoplasmic tail of the CaSR play very important roles in maintaining surface expression of the receptor, as assessed by both a biotin protection assay and a dual fluorescence antibody staining assay. Our results support a model (Fig. 7) in which high [Ca²⁺]_o-evoked increases of cytosolic calcium trigger stoichiometric binding of CaM to the C terminus of CaSR (aa 871–898) to stabilize the surface expression of the receptor and reduce its internalization. Such an interaction appears to be critical for maintaining a proper intracellular Ca²⁺ response to changes in extracellular Ca²⁺ in terms of the magnitude of the response, EC₅₀ for [Ca²⁺]_o and oscillation frequency. Moreover, binding of CaM may also sterically interfere with phosphorylation of the CaSR by PKC, which is known to reduce the coupling of the receptor to PLC and signaling via [Ca²⁺]_i. The relative amount of CaM binding *versus* PKC phosphorylation of Thr-888 likely has an important impact on the efficiency of signal transduction by the CaSR, at least in [Ca²⁺]_i signaling. Nevertheless, we observed two cases in which the behavior of the mutants contradict the proposed model. For example, the mutant T888V, which binds tightly to CaM without any possibility of phosphorylation by PKC, is expected to promote maximal oscillation frequency. However, T888V exhibits very slow oscillations. In the second case, the 3E1 (T888E) mutant pseudophosphorylates the CaSR at residue 888 and is anticipated to promote receptor internalization. This, however, was not observed under our experimental conditions. It is likely due to the fact that this mutant still retains the ability to weakly interact with CaM, thus counteracting the effect of pseu-

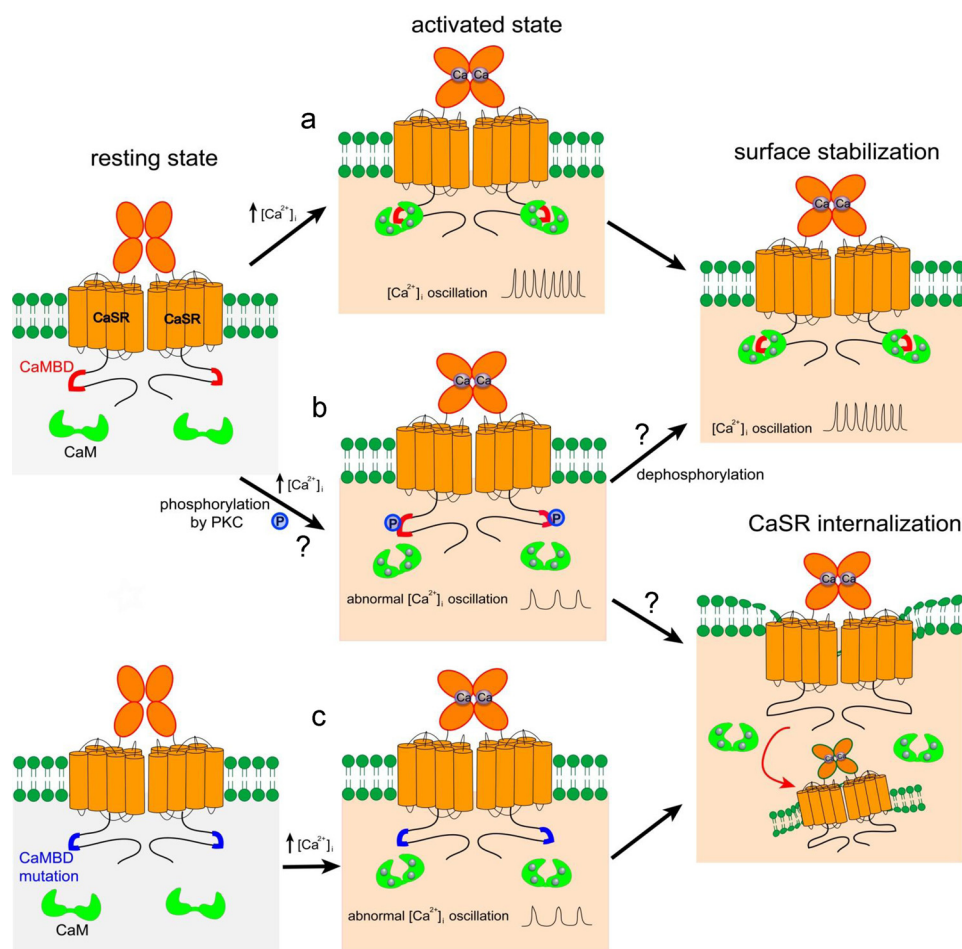


FIGURE 7. A working model of CaM and CaSR interaction. Our results support a model in which an increase of cytosolic calcium triggers CaM (green) to stoichiometrically bind to the C-terminal CaMBD (aa 871–898, highlighted in red) of CaSR to stabilize the surface expression of the receptor and reduce its internalization (panel a). Such an interaction, and perhaps more direct actions of CaM binding to the CaSR on the signaling of the receptor, appears to be critical for maintaining a proper intracellular Ca²⁺ response to changes in extracellular Ca²⁺, in terms of magnitude of the response, EC₅₀ for [Ca²⁺]_o, and oscillation frequency. Mutations within the CaMBD (blue, panel c) that abrogate CaM-target interaction cause enhanced internalization of CaSR. Adding complexity to this scenario, phosphorylation of Thr-888 within the CaMBD impairs its interaction with CaM. It is likely that the reversible phosphorylation of this site might serve as a switch between CaM-mediated effects when this residue is not phosphorylated (panel a) and PKC-mediated effects when phosphorylation occurs (panel b). More extensive studies are required to further determine the explicit mechanistic details.

dophosphorylation. Further structural and functional studies are needed to unravel the confounding effects of phosphorylation and Ca²⁺-dependent association of CaM with CaSR. Moreover, additional studies are needed to investigate the role of CaM in regulating the function of cells in which the CaSR is expressed endogenously as well as its regulation of other CaSR signaling pathways. Unfortunately, there are no cell lines of parathyroid cells, which express the highest level of the receptor in the body, and it is not clear how closely various CaSR-expressing cell lines mimic the normal function of the cells from which they were derived.

There are a few examples of modulation of GPCR signaling by their direct association with CaM. CaM has been reported to directly interact with the dopamine D2 receptor (41), serotonin 5-hydroxytryptamine receptors (42), and mGluRs (15). A 1–14 class of CaM-binding domain in the C terminus of mGluR7a has been identified by several groups (15), which can be aligned well with the predicted CaMBD in CaSR (Fig. 1). It has been

found that phosphorylation of Ser-862 in mGluR7a may inhibit CaM binding by interatomic repulsion. In addition, CaM dynamically regulates the trafficking of mGluR5 and is directly linked with the PKC phosphorylation at Ser-901. Blocking the PKC phosphorylation of Ser-901, and thus ensuring the interaction between CaM and mGluR5, has been shown to prolong Ca²⁺ oscillations. It is conceivable that a similar phosphorylation/dephosphorylation mechanism would apply to the CaM-CaSR association and contribute to the observed effects on Ca²⁺ oscillations, as noted above.

Overall, our studies on the interaction between CaM and CaSR provide novel insights into the mechanisms underlying the cross-talk between extra- and intracellular Ca²⁺ signaling. We have revealed a Ca²⁺-dependent stoichiometric interaction between CaM and a CaM-binding domain located at the C terminus of CaSR (aa 871–898). Substitution of the predicted hydrophobic residues with glutamates at proposed anchoring positions 1, 8, and/or 14 abolishes the interaction between CaM and CaSR and concomitantly decreases the magnitude and apparent affinity of the Ca²⁺ responses to [Ca²⁺]_o and perturbs receptor-evoked Ca²⁺ oscillation frequency. Thus, the interaction between CaM and CaSR may regulate the function of the receptor by positively modulating the [Ca²⁺]_i

response to the external Ca²⁺ level and by maintaining an appropriate Ca²⁺ oscillation frequency, effects that are antagonized by phosphorylation of Thr-888.

Acknowledgments—We thank Dan Adams for help in preparation of this manuscript and Dr. Mei Bai, Dr. Aldebaran Hofer, and other members of the Yang group for helpful suggestions.

REFERENCES

1. Brown, E. M., Gamba, G., Riccardi, D., Lombardi, M., Butters, R., Kifor, O., Sun, A., Hediger, M. A., Lytton, J., and Hebert, S. C. (1993) *Nature* **366**, 575–580
2. Brown, E. M., Pollak, M., and Hebert, S. C. (1998) *Annu. Rev. Med.* **49**, 15–29
3. Thakker, R. V. (2004) *Cell Calcium* **35**, 275–282
4. Chang, W., and Shoback, D. (2004) *Cell Calcium* **35**, 183–196
5. Ward, D. T. (2004) *Cell Calcium* **35**, 217–228
6. Huang, C., and Miller, R. T. (2007) *J. Cell Mol. Med.* **11**, 923–934
7. Zhang, M., and Breitwieser, G. E. (2005) *J. Biol. Chem.* **280**, 11140–11146

8. Ye, C. P., Yamaguchi, T., Chattopadhyay, N., Sanders, J. L., Vassilev, P. M., and Brown, E. M. (2000) *Bone* **27**, 21–27
9. Huang, Y., and Breitwieser, G. E. (2007) *J. Biol. Chem.* **282**, 9517–9525
10. Ray, K., Fan, G. F., Goldsmith, P. K., and Spiegel, A. M. (1997) *J. Biol. Chem.* **272**, 31355–31361
11. Bai, M., Janicic, N., Trivedi, S., Quinn, S. J., Cole, D. E., Brown, E. M., and Hendy, G. N. (1997) *J. Clin. Invest.* **99**, 1917–1925
12. Lienhardt, A., Garabédian, M., Bai, M., Sinding, C., Zhang, Z., Lagarde, J. P., Boulesteix, J., Rigaud, M., Brown, E. M., and Kottler, M. L. (2000) *J. Clin. Endocrinol. Metab.* **85**, 1695–1702
13. Kubokawa, K., Miyashita, T., Nagasawa, H., and Kubo, Y. (1996) *FEBS Lett.* **392**, 71–76
14. Enz, R. (2002) *FEBS Lett.* **514**, 184–188
15. O'Connor, V., El Far, O., Boffill-Cardona, E., Nanoff, C., Freissmuth, M., Karschin, A., Airas, J. M., Betz, H., and Boehm, S. (1999) *Science* **286**, 1180–1184
16. Lee, J. H., Lee, J., Choi, K. Y., Hepp, R., Lee, J. Y., Lim, M. K., Chatani-Hinze, M., Roche, P. A., Kim, D. G., Ahn, Y. S., Kim, C. H., and Roche, K. W. (2008) *Proc. Natl. Acad. Sci. U.S.A.* **105**, 12575–12580
17. Yap, K. L., Kim, J., Truong, K., Sherman, M., Yuan, T., and Ikura, M. (2000) *J. Struct. Funct. Genomics* **1**, 8–14
18. Huang, Y., Zhou, Y., Yang, W., Butters, R., Lee, H. W., Li, S., Castiblanco, A., Brown, E. M., and Yang, J. J. (2007) *J. Biol. Chem.* **282**, 19000–19010
19. Liu, Y., and Prestegard, J. H. (2009) *J. Magn. Reson.* **200**, 109–118
20. Valafar, H., Mayer, K. L., Bougault, C. M., LeBlond, P. D., Jenney, F. E., Jr., Brereton, P. S., Adams, M. W., and Prestegard, J. H. (2004) *J. Struct. Funct. Genomics* **5**, 241–254
21. Zhou, Y., Yang, W., Lurtz, M. M., Chen, Y., Jiang, J., Huang, Y., Louis, C. F., and Yang, J. J. (2009) *Biophys. J.* **96**, 2832–2848
22. Bai, M., Trivedi, S., and Brown, E. M. (1998) *J. Biol. Chem.* **273**, 23605–23610
23. Zhou, Y., Yang, W., Lurtz, M. M., Ye, Y., Huang, Y., Lee, H. W., Chen, Y., Louis, C. F., and Yang, J. J. (2007) *J. Biol. Chem.* **282**, 35005–35017
24. Roth, S. M., Schneider, D. M., Strobel, L. A., VanBerkum, M. F., Means, A. R., and Wand, A. J. (1991) *Biochemistry* **30**, 10078–10084
25. Prestegard, J. H., Bougault, C. M., and Kishore, A. I. (2004) *Chem. Rev.* **104**, 3519–3540
26. Contessa, G. M., Orsale, M., Melino, S., Torre, V., Paci, M., Desideri, A., and Cicero, D. O. (2005) *J. Biomol. NMR* **31**, 185–199
27. Mal, T. K., Skrynnikov, N. R., Yap, K. L., Kay, L. E., and Ikura, M. (2002) *Biochemistry* **41**, 12899–12906
28. Aoyagi, M., Arvai, A. S., Tainer, J. A., and Getzoff, E. D. (2003) *EMBO J.* **22**, 766–775
29. Clapperton, J. A., Martin, S. R., Smerdon, S. J., Gamblin, S. J., and Bayley, P. M. (2002) *Biochemistry* **41**, 14669–14679
30. Ikura, M., Barbato, G., Klee, C. B., and Bax, A. (1992) *Cell Calcium* **13**, 391–400
31. Davies, S. L., Ozawa, A., McCormick, W. D., Dvorak, M. M., and Ward, D. T. (2007) *J. Biol. Chem.* **282**, 15048–15056
32. Breitwieser, G. E. (2006) *Curr. Top. Dev. Biol.* **73**, 85–114
33. Breitwieser, G. E., and Gama, L. (2001) *Am. J. Physiol. Cell Physiol.* **280**, C1412–C1421
34. Reyes-Ibarra, A. P., Garcia-Regalado, A., Ramirez-Rangel, I., Esparza-Silva, A. L., Valadez-Sanchez, M., Vazquez-Prado, J., and Reyes-Cruz, G. (2007) *Mol. Endocrinol.* **21**, 1394–1407
35. Crivici, A., and Ikura, M. (1995) *Annu. Rev. Biophys. Biomol. Struct.* **24**, 85–116
36. Hoeflich, K. P., and Ikura, M. (2002) *Cell* **108**, 739–742
37. Ray, J. M., Squires, P. E., Curtis, S. B., Meloche, M. R., and Buchan, A. M. (1997) *J. Clin. Invest.* **99**, 2328–2333
38. Bai, M., Trivedi, S., Lane, C. R., Yang, Y., Quinn, S. J., and Brown, E. M. (1998) *J. Biol. Chem.* **273**, 21267–21275
39. Chang, W., Pratt, S., Chen, T. H., Bourguignon, L., and Shoback, D. (2001) *J. Biol. Chem.* **276**, 44129–44136
40. Bouschet, T., Martin, S., and Henley, J. M. (2008) *Trends Pharmacol. Sci.* **29**, 633–639
41. Boffill-Cardona, E., Kudlacek, O., Yang, Q., Ahorn, H., Freissmuth, M., and Nanoff, C. (2000) *J. Biol. Chem.* **275**, 32672–32680
42. Turner, J. H., Gelasco, A. K., and Raymond, J. R. (2004) *J. Biol. Chem.* **279**, 17027–17037
43. Brokx, R. D., Lopez, M. M., Vogel, H. J., and Makhatadze, G. I. (2001) *J. Biol. Chem.* **276**, 14083–14091